AAS 09-257

OPTIMIZATION OF SPACECRAFT TRAJECTORIES: A METHOD COMBINING INVARIANT MANIFOLD TECHNIQUES AND DISCRETE MECHANICS AND OPTIMAL CONTROL

Ashley Moore[*], Sina Ober-Blöbaum[†], and Jerrold E. Marsden[‡]

A mission design technique that uses invariant manifold techniques together with the optimal control algorithm DMOC produces locally optimal, low ΔV trajectories. Previously, invariant manifolds of the planar circular restricted three body problem (PCR3BP) have been used to design trajectories with relatively small ΔV. Using local optimal control methods, specifically DMOC, it is possible to reduce the ΔV even further. This method is tested on a trajectory which begins in Earth orbit and ends in ballistic capture at the Moon. DMOC produces locally optimal trajectories with much smaller total ΔV applied in a distributed way along the trajectory. Additionally, DMOC allows for variable flight times, leading to smaller ΔV necessary for lunar orbit insertion. Results from different Earth to Moon missions are presented in table form to show how the DMOC results fit in with actual missions and different trajectory types. The ΔV of the DMOC results are, on average, 23%-25% better than the ΔV of trajectories produced using a Hohmann transfer.

INTRODUCTION

Many techniques focus on the design of spacecraft trajectories. Numerous successful NASA mission trajectories were designed using 2-body patched conics. Furthermore, invariant manifolds of the planar circular restricted 3-body problem (PCR3BP) have been used to find energy efficient trajectories that follow the natural dynamics of the solar system from one region of space to another. The 3-body problem is well understood and allows for the design of complicated trajectories not possible using patched conics. What about the design of a trajectory in the 4-body problem? Since the N-body problem is notoriously difficult to solve, much work has focused on patching multiple 3-body systems together, which typically include impulsive control at the intersection of the invariant manifolds of the two systems. The work of this paper aims to extend this method, to solve the problem using 4-body dynamics and to apply local optimal control throughout the trajectory, instead of impulsive control concentrated at the intersection. Does the application of small ΔV throughout the trajectory, designed using an optimal control scheme, minimize the total ΔV? This paper seeks to answer that question by combining invariant manifold techniques in the PCR3BP with the optimal control algorithm DMOC (Discrete Mechanics and Optimal Control).

Since the 1950's countless missions have targeted the moon, sending spacecraft along trajectories for fly-bys, lunar observation orbits, and both manned and unmanned lunar landings. More

[*]Graduate Student, Control and Dynamical Systems, California Institute of Technology, MC 107-81, Pasadena, CA 91125, USA.

[†]Postdoctoral Scholar, Control and Dynamical Systems, California Institute of Technology, MC 107-81, Pasadena, CA 91125, USA.

[‡]Carl F. Braun Professor of Engineering and CDS, Control and Dynamical Systems, California Institute of Technology, MC 107-81, Pasadena, CA 91125, USA.

recently, propulsion technology and design techniques, including the use of invariant manifolds, have facilitated the design of creative, fuel efficient trajectories. For example, in an effort to salvage Japan's Hiten mission, Belbruno and Miller (1993)[1,2] designed an unusual and fuel efficient trajectory utilizing invariant manifolds that resulted in ballistic capture at the Moon. In addition, ESA's SMART-1, Camino et. al (2005),[3] was launched in 2003 to demonstrate the potential use of ion propulsion for future interplanetary and deep space missions. The sustained thrust provided by the ion thruster allowed the spacecraft to spiral out from an elliptical orbit around the Earth to the Moon and then spiral in for lunar capture. This paper focuses on the transfer from the Earth to the Moon along a trajectory that uses invariant manifolds, like Hiten, and control applied throughout the entire trajectory, like SMART-1.

Invariant Manifold Techniques

Invariant manifolds are tube-like structures along which a spacecraft may travel using no energy. The manifolds can lead, for example, to periodic orbits around the Lagrange points of the PCR3BP. Conley (1968)[4] and McGeehee (1969)[5] were the first to study the orbit structures around the L_1 and L_2 Lagrange points. The transport made possible by invariant manifolds has been exploited for several different trajectories. For example, the work of Belbruno and Miller (1993)[1] mentioned above presents the idea of patching these invariant manifold tubes together to effect transfer between the Earth and the Moon. Gómez et al. (1993)[6] studies transfer from the Earth to a Halo orbit about the L_1 equilibrium point of the Sun-Earth 3-body system. Invariant manifolds are also used by Gómez et al. (2001)[7] to design a trajectory that tours the Moons of Jupiter. Koon et al. (1999),[8] Gómez et al. (2004),[9] and Dellnitz et al. (2001)[10] explain how heteroclinic connections between libration orbits enable the existence of a trajectory like the one used by the Genesis mission. This work focuses on the trajectory studied in Koon et al. (2001 and 2000)[11,12] and Belbruno and Miller (1993)[1] which follows invariant manifolds to transfer from the Earth to the Moon.

Invariant manifold techniques usually only provide trajectories for uncontrolled spacecraft. Rather impulsive control is used at the intersection between different invariant manifolds. An extension of invariant manifold techniques in order to account for a continuously applied control force is presented in Dellnitz et al. (2006)[13] and applied to design a trajectory from Earth to Venus and from Earth to L_2,[14] respectively. However, so far these techniques are only computationally reasonable for a constant one-dimensional control force. Instead we are interested in a time-dependent control law influencing all degrees of freedom of the spacecraft in each time point which are optimal w.r.t. a certain goal. Therefore, the application of a local optimal control scheme is indispensible for the design of trajectories with more complex control laws. Thereby, the computed thrustless trajectories designed with the help of invariant manifold techniques serve as initial guess for the optimization of the controlled model.

Local Optimal Control

Optimal control methods have been applied to many different space related problems already. For example, in Junge et al. (2005),[15] DMOC is used to optimally raise a spacecraft in circular orbit to an orbit of greater radius and to reconfigure a group of hovercraft. Trajectory design in the 4-body problem is a natural extension for DMOC. There are many local optimal control methods and a short overview is warranted. In principle, there are indirect and direct local optimal control methods; here we will focus on direct methods, where the optimal control problem is transformed into a constrained optimization problem by an appropriate discretization of the differential system

under consideration. Some well-known direct methods include shooting (see e.g. Stoer and Bulirsch (1993),[16] Kraft (1985),[17] Hicks and Ray (1971)[18]), multiple shooting (see e.g. Deuflhard (1974),[19] Book and Plitt (1984),[20] Leineweber et al. (2003)[21]), and collocation methods (see e.g. von Stryk (1993),[22] Biegler (1984)[23]). These methods rely on a direct integration of the associated ordinary differential equations or on its fulfilment at certain grid points, see also Betts (1998)[24] and Binder et al. (2001)[25] for an overview of the current state of the art. In contrast to these previously mentioned methods, the recently developed DMOC (*Discrete Mechanics and Optimal Control*) (Ober-Blöbaum (2008)[26] and Junge et al. (2005)[15]) is based on the discretization of the variational structure of the mechanical system directly. The discretization of the Lagrange-d'Alembert principle[27] leads to structure preserving time stepping equations which serve as equality constraints for the resulting finite dimensional nonlinear optimization problem. This problem can be solved by standard nonlinear optimization techniques such as sequential quadratic programming (see e.g. Gill et al. (1997),[28] Gill et al. (2000),[29] Powell (1978)[30] and Han (1976)[31]).

Shoot the Moon

The method presented in this article is tested on the Shoot the Moon problem, presented by Koon, Lo, Marsden and Ross.[12] The Shoot the Moon problem computes a trajectory which begins in low Earth orbit, travels along the invariant manifolds of the Sun-Earth and Earth-Moon PCR3BPs, and ends in orbit about the Moon. The trajectory presented in Koon et al. (2000)[12] requires a total ΔV of approximately 3,245 m/s which consists of two parts: an initial thrust to escape Earth orbit (3,211 m/s), and a thrust applied mid-course (34 m/s). This trajectory results in ballistic capture at the Moon. The spacecraft is not, however, inserted into orbit about the Moon. The results presented in this article include a ΔV applied at the Moon for this orbit insertion. A trajectory similar to that of Koon et al. (2000)[12] is produced and used as an initial guess for DMOC, which searches for an optimal trajectory in the 4-body system, applying control throughout the trajectory to decrease the total ΔV.

Organization of the Article

The remainder of this article is organized as follows: the Problem Formulation and Methods section presents the basics necessary to understand the problem and the methods in use. Specifically, the theory is described in subsections Trajectory Design Using Invariant Manifolds of the 3-Body Problem, Bicircular 4-Body Model, and Discrete Mechanics and Optimal Control. The Optimization Procedure section delineates the specific process used to implement DMOC using an initial guess derived from a trajectory designed using the Invariant Manifolds of the 3-body problem. This section is followed by the Optimization Results, Conclusions, and Future Work.

PROBLEM FORMULATION AND METHODS

The fundamental theory and the problem description that form the basis for this work are presented in this section including invariant manifolds of planar restricted 3-body problem, the bicircular 4-body model, and DMOC.

Trajectory Design Using Invariant Manifolds of the 3-Body Problem

The Shoot the Moon problem begins with two coupled planar circular restricted 3-body problems.[12] The geometry of the PCR3BP is shown in Figure 1. For each PCR3BP, the motion of a

body is described under the influence of two main bodies, either the Sun and the Earth in the Sun-Earth system or the Earth and the Moon for the Earth-Moon system. Each system is described in a rotating coordinate frame and mass is normalized with the mass parameter

$$\mu = \frac{M_2}{M_1 + M_2} \tag{1}$$

where $M_1 > M_2$. For example, in the Sun-Earth 3-body system, M_1 denotes the mass of the Sun and M_2 denotes the mass of the Earth. The normalized mass of the larger body is denoted by $m_1 = 1 - \mu$, and the normalized mass of the smaller body is $m_2 = \mu$. The two primary bodies rotate in circular, planar orbits about their common center of mass at the origin. The third body, the spacecraft, is assumed to have infinitesimal mass. The primary bodies, m_1 and m_2, are positioned at $(-\mu, 0)$ and $(1-\mu, 0)$, respectively. The equations of motion for the PCR3BP are

$$\ddot{x} - 2\dot{y} = \frac{\partial \Omega}{\partial x} \tag{2}$$

$$\ddot{y} + 2\dot{x} = \frac{\partial \Omega}{\partial y} \tag{3}$$

where

$$\Omega = \frac{x^2 + y^2}{2} + \frac{1-\mu}{\sqrt{(x+\mu)^2 + y^2}} + \frac{\mu}{\sqrt{(x-1+\mu)^2 + y^2}} \tag{4}$$

The system, Eq. (2)-(4), has five equilibrium points $L_1, \ldots, L_5$ (cf. Figure 1); the unstable L_2 point is of interest for this work.

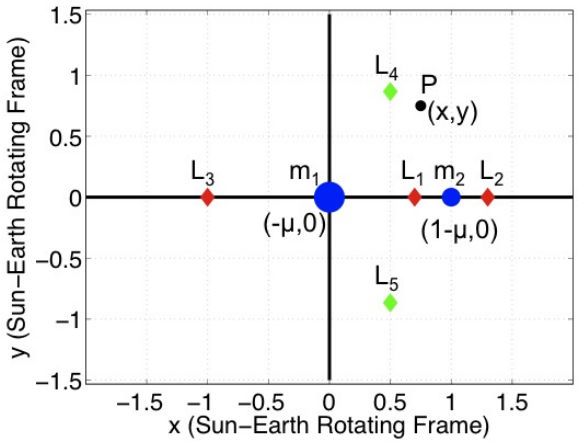

Figure 1 Geometry of PCR3BP in Sun-Earth rotating frame with two primary masses, m_1 and m_2, and Lagrange points $\{L_i\}_{i=1}^5$.

Stable and unstable manifolds emanate from the periodic orbit of the L_2 Lagrange point, shown in Figure 2. These manifold tubes control transport into and out of the region around m_2.[12] The unstable manifold of the Sun-Earth system leads away from the periodic orbit around L_2, while the stable manifold leads towards the periodic orbit. Only the stable manifold of the Earth-Moon system is shown because this manifold controls transport from an exterior region to the Moon.

The equations of motion for the PCR3BP are Hamiltonian and time independent, so there exists the following energy integral.

$$E = \frac{1}{2}(\dot{x}^2 + \dot{y}^2) - \Omega(x, y) \tag{5}$$

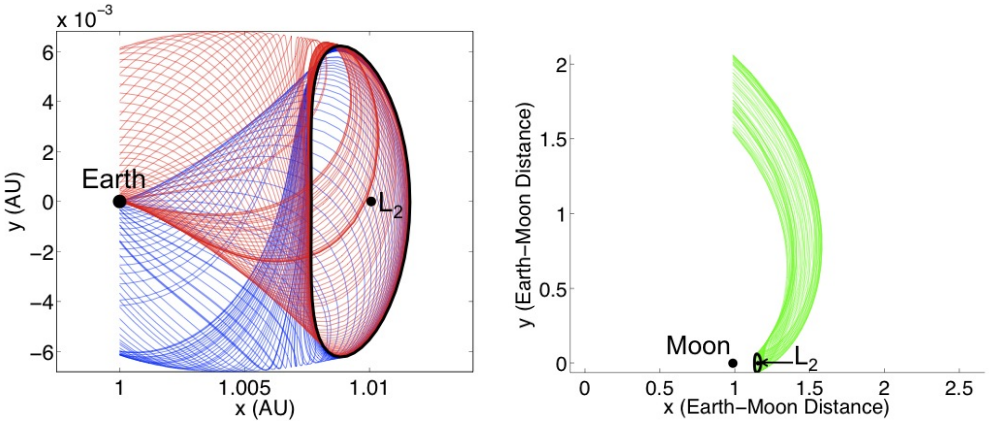

Figure 2 Manifolds emanate from the periodic orbit about L_2 (a) Stable (bottom) and Unstable (top) manifolds of the Sun-Earth L_2 Lagrange point. (b) Stable manifold of Earth-Moon L_2 Lagrange point.

The phase space of the PCR3BP may be divided into regions of possible and forbidden motion based on this energy.[32] There are five possible cases, with the first four cases shown in Figure 3. Each plot shows the Hill's region, a projection of the energy surface $\mathcal{M}(\mu, e) = \{(x, y, \dot{x}, \dot{y}) | E(x, y, \dot{x}, \dot{y}) = e\}$ onto configuration space, for a particular energy level. The cases are distinguished by the critical energy $\{E_i\}_{i=1}^{5}$, which represents the energy of a particle at rest at the Lagrange point$\{L_i\}_{i=1}^{5}$. For example, if the energy of the spacecraft is greater than E_2 but less than E_3, it is energically possible for the spacecraft to move through the manifold tubes from the region surrounding m_2 to an exterior region and vice versa, as shown in plot (c) of Figure 3. Furthermore, this energy is important for transfer between manifolds of different PCR3BPs.

To achieve transfer between the Earth and Moon using the invariant manifolds, a first step is to locate the intersection of the unstable Sun-Earth manifold with the stable Earth-Moon manifold. A Poincaré section is used to find this intersection in the Sun-Earth rotating frame. The phase of the Earth-Moon frame with respect to the Sun-Earth frame can be adjusted until a suitable intersection is found.

Using the Poincaré section, shown on the right hand side of Figure 4, a patch point is selected that falls within the stable manifold of the Earth-Moon system and outside the unstable manifold of the Sun-Earth system. From the Poincaré section, the patch point includes x, y, and $\dot{y}$. The x-velocity, $\dot{x}$, is selected so that the energy integral at the patch point equals that of the desired manifold. Forward integration of the conditions at the patch point (x, y, $\dot{x}$, $\dot{y}$) leads to a trajectory that flows through the stable Earth-Moon manifold and ends near the Moon. The same initial conditions are modified slightly in $\dot{x}$ and $\dot{y}$ and integrated backwards, generating a trajectory that hugs the unstable Sun-Earth manifold and then twists, targeting back to the Earth. The modification in the velocity ensures that the energy of the spacecraft is at the appropriate level to travel along the Sun-Earth manifold in the desired manner. The Sun-Earth and Earth-Moon trajectories are patched together to form a trajectory which begins at the Earth and ends at the Moon. Note that at the patch point, the energy is discontinuous; therefore, a ΔV is necessary to jump from the energy level of the Sun-Earth manifold to the energy of the Earth-Moon manifold. For mathematical details about this process, we refer to Koon et al. (2001)[12] and Ross (2004).[32] The trajectory is shown in Figure 5;

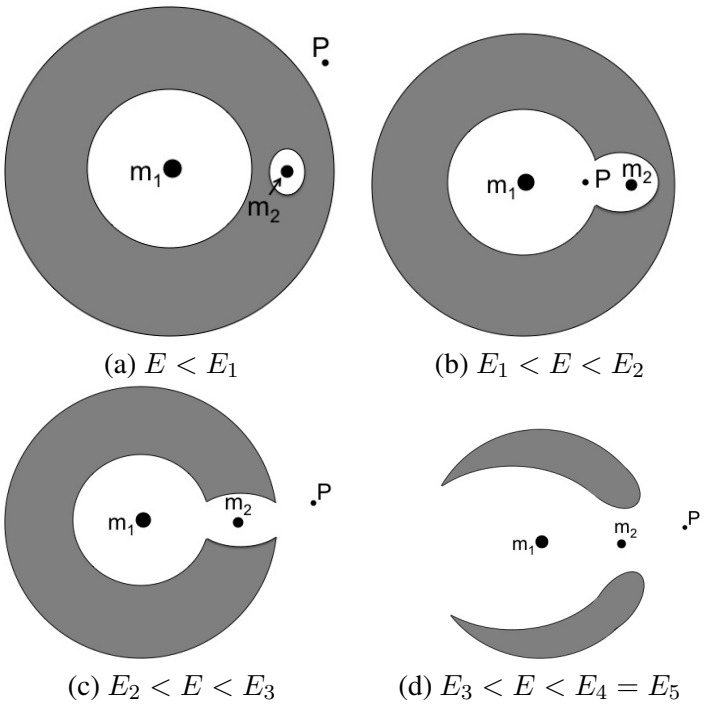

(a) $E < E_1$ (b) $E_1 < E < E_2$

(c) $E_2 < E < E_3$ (d) $E_3 < E < E_4 = E_5$

Figure 3 Regions of possible motion: (a) P cannot move between m_1 and m_2 (b) P can move between m_1 and m_2 via L_1 (c) P may move from m_1 to m_2 to exterior region via L_1 and L_2 (d) P may travel past m_1 to exterior region via L_3. Case 5, $E > E_5$, is not shown: P may move freely in x-y plane.

it begins in an 315 km radius circular orbit about the Earth and ends in an $3.82 \cdot 10^5$ km circular orbit about the Moon. An initial thrust of 3,246.9 m/s is required to escape Earth orbit along the trajectory, a mid-course ΔV of 124.3 m/s is applied at the patch point, and a final ΔV of 3,024.0 m/s is required to settle into a permanent circular orbit at the Moon.

Bicircular 4-Body Model

The trajectory created in the previous section is valid for the patched 3-body problem only. We want to optimize the trajectory in the 4-body problem. Therefore, it is necessary to create a new trajectory, beginning at the same patch point and integrating forwards and backwards using 4-body dynamics. The bicircular 4-body model describes the dynamics of the Sun, Earth, Moon, and spacecraft as follows. The Earth and Moon rotate in planar circular motion about their common center of mass. Then, the barycenter of the Earth-Moon system and the Sun rotate in planar circular motion about the common center of mass of the three bodies. As before, the mass of the spacecraft is negligible. Figure 6 shows the geometry of this 4-body model. The equations of motion for this model in Sun-Earth rotating coordinates are[32]

$$\ddot{x} - 2\dot{y} = \frac{\partial \Omega}{\partial x} \tag{6}$$

$$\ddot{y} + 2\dot{x} = \frac{\partial \Omega}{\partial y} \tag{7}$$

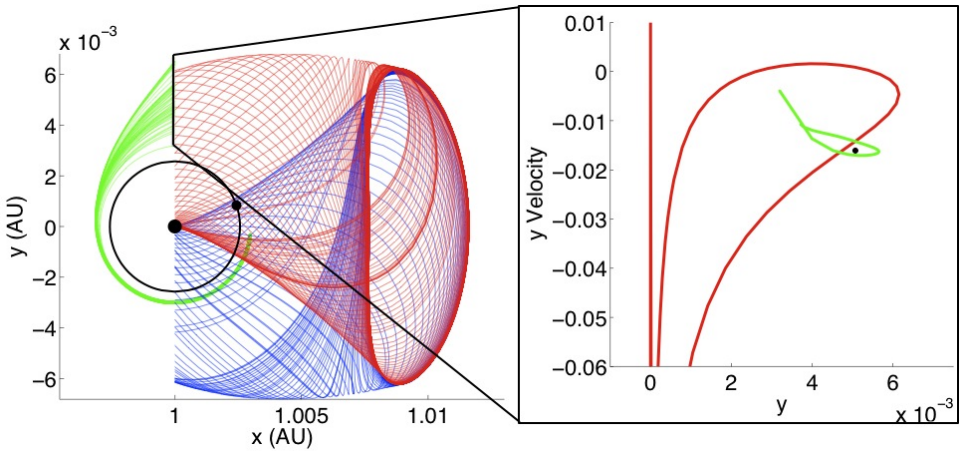

Figure 4 Poincaré section showing the intersection of the Sun-Earth unstable manifold with the Earth-Moon stable manifold. The patch point of the manifolds is chosen inside the stable Earth-Moon manifold and outside unstable Sun-Earth manifold.

where

$$\Omega = \frac{x^2+y^2}{2} + \frac{\mu_S}{\sqrt{(x-x_S)^2+y^2}} + \frac{\mu_E}{\sqrt{(x-x_E)^2+y^2}} + \frac{\mu_M}{\sqrt{(x-x_M)^2+(y-y_M)^2}} \tag{8}$$

and μ_S, μ_E, and μ_M are the normalized mass of the Sun, Earth, and Moon, respectively, given by

$$\mu_S = 1-\mu \tag{9}$$

$$\mu_E = \mu \tag{10}$$

$$\mu_M = \frac{M_M}{M_M+M_E+M_S} = 3.734\cdot 10^{-8} \tag{11}$$

and

$$\mu = \frac{M_E+M_M}{M_E+M_M+M_S} = 3.036\cdot 10^{-6} \tag{12}$$

Note that M_i, $i = E, M, S$, denotes the body's mass in kg. Also, x_S, x_E, and x_M represent the x-position of the Sun, Earth, and Moon respectively, and y_M is the y-position of the Moon (the Sun and Earth lie on the x-axis). The position of the Moon is a function of time given by

$$\theta_M = \omega_M t + \theta_{M0} \tag{13}$$

$$x_M = a_M \cos\theta_M \tag{14}$$

$$y_M = a_M \sin\theta_M \tag{15}$$

where t is time, θ_{M0} is the initial angle of the Moon with respect to the x-axis in the Sun-Earth rotating frame, $a_M = 2.573\cdot 10^{-3}$ is the normalized radius of the Moon's circular orbit, and $\omega_M = 12.369$ is the normalized rotation rate of the Moon.

Beginning with the same initial conditions from the patch point, $\dot{x}$ and $\dot{y}$ are modified slightly and integrated using the bicircular 4-body model. The modification is necessary due to the differences between the dynamics of the PCR3BP and the bicircular 4-body problem. The point is modified differently for the Sun-Earth section and the Earth-Moon section because of the energy differences

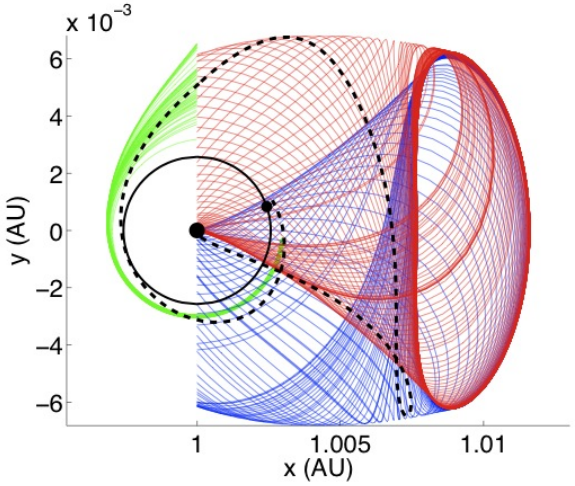

Figure 5 Trajectory in 3-body problem (in Sun-Earth Rotating coordinates), begins near the Earth, hugs the Sun-Earth unstable manifold towards the periodic orbit of L_2. It twists and then intersects the stable manifold of the Earth-Moon system, following that manifold to the realm of the Moon.

between the manifolds of the two systems. Thus, the initial conditions denoted by IC_{SE} and IC_{EM}, respectively, can be expressed as

$$IC_{SE} = \begin{bmatrix} x & y & \dot{x} + \Delta\dot{x}_{SE} & \dot{y} + \Delta\dot{y}_{SE} \end{bmatrix} \quad (16)$$

$$IC_{EM} = \begin{bmatrix} x & y & \dot{x} + \Delta\dot{x}_{EM} & \dot{y} + \Delta\dot{y}_{EM} \end{bmatrix} \quad (17)$$

IC_{SE} is integrated backwards to generate the Sun-Earth portion of the trajectory, and IC_{EM} is integrated forwards to generate the Earth-Moon portion of the trajectory. Note, that the Δ's are adjusted until a good trajectory is found: a trajectory which begins and ends at a desired radius about the Earth and Moon, respectively. Note that the initial and final momentum values may not be favorable. DMOC adjusts these momentum values according to the specified constraints and cost function during optimization. This trajectory serves as the initial guess for DMOC.

Discrete Mechanics and Optimal Control

In order to compute a trajectory with minimal fuel consumption, we make use of local optimal control techniques. DMOC[15,26] is an optimal control scheme that is based on a direct discretization of the Lagrange-d'Alembert principle of the mechanical system. The discretization leads to the forced discrete Euler-Lagrange equations which are used as optimization constraints for a given cost function. The resulting restricted optimization problem is solved with an SQP solver.

For convenience we briefly summarize the basic idea. Consider a mechanical system to be moved along a curve $q(t) \in Q$ during the time interval $t \in [0, T]$ from an initial state $(q^0, \dot{q}^0)$ to a final state $(q^T, \dot{q}^T)$ under the influence of a force $f(q(t), \dot{q}(t), u(t))$ where $u(t) \in U$ is a control parameter. The curves q and u are chosen to minimize a given cost functional

$$J(q, \dot{q}, u) = \int_0^T C(q(t), \dot{q}(t), f(q(t), \dot{q}(t), u(t)))\, dt \quad (18)$$

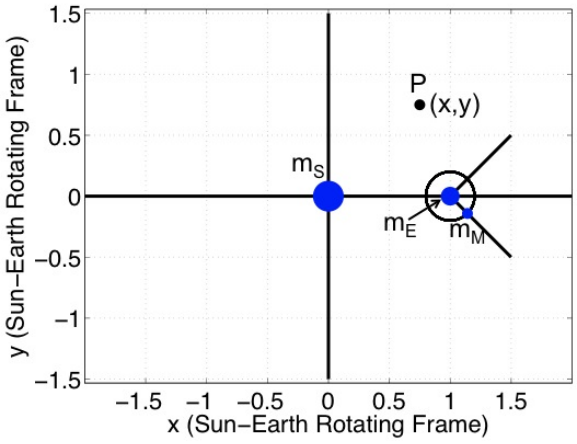

Figure 6 Bicircular 4-Body Model: geometry in the Sun-Earth rotating frame with three primary masses, m_S, m_E, and m_M, and spacecraft, P. The Moon rotates relative to the Sun-Earth rotating frame, which is stationary.

subject to the condition that the system satisfies the Lagrange-d'Alembert prcinple, which states that

$$\delta \int_0^T L(q(t), \dot{q}(t))\, dt + \int_0^1 f(q(t), \dot{q}(t), u(t)) \cdot \delta q(t)\, dt = 0 \tag{19}$$

for all variations δq with $\delta q(0) = \delta q(T) = 0$, where $L : TQ \to \mathbb{R}$ is the Lagrangian consisting of the kinetic minus potential energy of the system.

The optimal control problem stated in Eq. (18) and Eq. (19) is now transformed into a finite dimensional constrained optimization problem using a global discretization of the states and the controls. We replace the state space TQ by $Q \times Q$ and consider the grid $\Delta t = \{t_k = kh \,|\, k = 0, \ldots, N\}$, $Nh = T$, where N is a positive integer and h the stepsize. We replace a path $q : [0, T] \to Q$ by a discrete path $q_d : \{t_k\}_{k=0}^N \to Q$, where we view $q_k = q_d(kh)$ as an approximation to $q(kh)$.[27,26] Similarly, we replace the control path $u : [0, T] \to U$ by a discrete one. To this end, we consider a refined grid $\Delta\tilde{t}$, generated via a set of control points $0 \le c_1 < \cdots < c_s \le 1$ as $\Delta\tilde{t} = \{t_{k\ell} = t_k + c_\ell h \,|\, k = 0, \ldots, N-1; \ell = 1, \ldots, s\}$. With this notation, the discrete control path is defined to be $u_d : \Delta\tilde{t} \to U$. We define the intermediate control samples u_k on $[t_k, t_{k+1}]$ as $u_k = (u_{k1}, \ldots, u_{ks}) \in U^s$ to be the values of the control parameters guiding the system from $q_k = q_d(t_k)$ to $q_{k+1} = q_d(t_{k+1})$, where $u_{kl} = u_d(t_{kl})$ for $l \in \{1, \ldots, s\}$.

Using an approximation of the action integral in Eq. (19) by a discrete Lagrangian $L_d : Q \times Q \to \mathbb{R}$,

$$L_d(q_k, q_{k+1}) \approx \int_{kh}^{(k+1)h} L(q(t), \dot{q}(t))\, dt$$

and discrete forces

$$f_k^- \cdot \delta q_k + f_k^+ \cdot \delta q_{k-1} \approx \int_{kh}^{(k+1)h} f(q(t), \dot{q}(t), u(t)) \cdot \delta q(t)\, dt$$

where the left and right discrete forces $f_k^\pm$ now depend on (q_k, q_{k+1}, u_k), we obtain the discrete Lagrange-d'Alembert principle, Eq. (20). Therefore, it is necessary to consider discrete paths

$\{q_k\}_{k=0}^N$ such that for all variations $\{\delta q_k\}_{k=0}^N$ with $\delta q_0 = \delta q_N = 0$, it is true that

$$\delta \sum_{k=0}^{N-1} L_d(q_k, q_{k+1}) + \sum_{k=0}^{N-1} \left(f_k^- \cdot \delta q_k + f_k^+ \cdot \delta q_{k+1} \right) = 0 \tag{20}$$

In the same manner, we obtain via an approximation of the cost functional Eq. (18), discrete cost functions C_d and J_d, respectively.

Then, the goal of the discrete constrained optimization problem is to minimize the discrete cost function

$$J_d(q_d, u_d) = \sum_{k=0}^{N-1} C_d(q_k, q_{k+1}, u_k) \tag{21}$$

subject to the constraints

$$\begin{aligned} q_0 &= q^0 && (22)\\ q_N &= q^T && (23)\\ D_2L(q^0, \dot{q}^0) + D_1L_d(q_0, q_1) + f_0^- &= 0 && (24)\\ D_2L_d(q_{k-1}, q_k) + D_1L_d(q_k, q_{k+1}) + f_{k-1}^+ + f_k^- &= 0 && (25)\\ -D_2L(q^T, \dot{q}^T) + D_2L_d(q_{N-1}, q_N) + f_{N-1}^+ &= 0 && (26) \end{aligned}$$

with $k = 1, ..., N-1$. The first two constraints require that the initial and final discrete positions match the continuous positions. The third and final constraints are the discrete momentum boundary conditions, and the fourth condition is the forced discrete Euler-Lagrange equation resulting from Eq. (20). Balancing accuracy and efficiency, we approximate the discrete cost function, C_d, the discrete Lagrangian, L_d, and the discrete forces with the midpoint rule and assume constant control parameters on each time interval with $l = 1$ and $c_1 = \frac{1}{2}$ as

$$C_d(q_k, q_{k+1}, u_k) = hC\left(\frac{q_{k+1} + q_k}{2}, \frac{q_{k+1} - q_k}{2}, u_k\right) \tag{27}$$

$$L_d(q_k, q_{k+1}) = hL\left(\frac{q_{k+1} + q_k}{2}, \frac{q_{k+1} - q_k}{h}\right) \tag{28}$$

$$f_k^- = f_k^+ = \frac{h}{2} f\left(\frac{q_{k+1} + q_k}{2}, \frac{q_{k+1} - q_k}{2}, u_k\right) \tag{29}$$

Eq. (21)-(26) describe a nonlinear optimization problem with equality constraints, which can be solved by standard optimization methods like SQP. Optionally, we can also include inequality constraints on states and controls.

OPTIMIZATION PROCEDURE

The optimization method can be broken into three parts: creation of the initial guess trajectory in the 4-body problem, computation of a feasible trajectory, and DMOC optimization. Each step of the process is performed using *Matlab*, and the SQP solver *fmincon* runs the optimization. The goal of the optimization is to produce a trajectory that begins in an approximately 200 km altitude orbit about the Earth and ends approximately 325 km from the Moon using minimal ΔV. As described before, an initial guess is found using the bicircular 4-body model.

Creation of Initial Guess

Two different initial guess trajectories are created using slightly different initial conditions, and are shown in Figure 7. The first trajectory (IG1) is a good initial guess for the DMOC optimization because it nearly fulfills the initial and final altitude requirements. The second guess trajectory (IG2) ends far from the Moon to test DMOC's ability to deal with a faulty initial guess. Table 1 shows the differences between these two trajectories. The ΔV described are impulsive ΔV which are applied at the first node to escape Earth orbit onto the trajectory (ΔV_E), at the patch point to jump from manifold to manifold (ΔV_{traj}), and at the final node to inject into circular orbit about the Moon (ΔV_M).

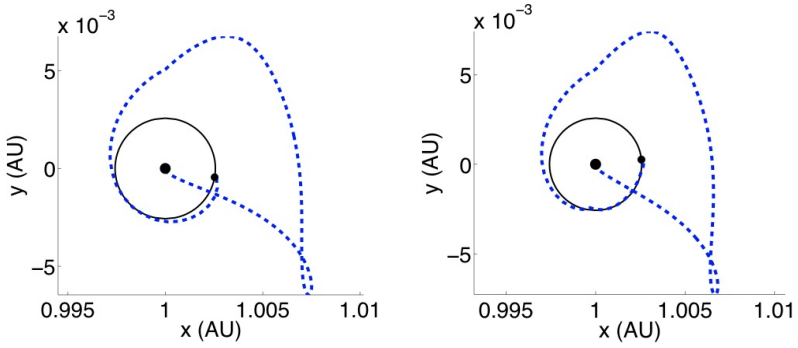

(a) (b)

Figure 7 Initial guess trajectories in the 4-body problem (a) IG1, Total $\Delta V = 5,281.8$ m/s with $\Delta V_{traj} = 197.2$ m/s (b) IG2, Total $\Delta V = 4,897.5$ m/s with $\Delta V_{traj} = 202.0$ m/s. ΔV_{traj} is applied at the patch point, shown in Figure 8.

Table 1. Details of Initial Guess Trajectories

	IG1	IG2
Initial Earth Orbit Altitude (km)	206.9	215.1
Final Moon Orbit Altitude (km)	326.8	16,228.0
Time of Flight (days)	175.5	178.8
Total ΔV (m/s)	5,281.8	4,897.5
ΔV_E (m/s)	3,216.0	3,222.7
ΔV_M (m/s)	1,868.7	1,472.8
ΔV_{traj} (m/s)	197.2	202.0
Number of nodes	271	259

For an initial guess trajectory, we use a constant step size between nodes for DMOC. However, the nonlinearity of the dynamics poses a problem. If a single step size is used throughout the trajectory, two scenarios are possible. First, if a medium step size is used, e.g. $\mathcal{O}(10^{-2})$, there are not enough nodes near the Earth and Moon to accurately capture the dynamics. On the other hand, if a sufficiently small step size is used, e.g. $\mathcal{O}(10^{-5})$, there are too many nodes for a reasonable computation time. To solve this problem, the trajectory is broken into m separate sections of uniform step size h_i with discrete paths $(q_i)_d$ and discrete control paths $(u_i)_d$, $i = 1, \ldots, m$. Then, when DMOC is applied, the position and velocity at the boundaries are enforced as additional constraints for the optimization problem. For example, the position and velocity of the final node of section 1 must equal that of the first node of section 2. Four sections are chosen as the ideal number to capture the dynamics in the fewest number of nodes. As shown in Figure 8, section 1 is nearest to the Earth,

section 2 covers a small section leading away from the Earth, section 3 covers the majority of the trajectory away from the influence of the Earth and Moon, and section 4 is near the Moon. For example, the step sizes used for IG1 are $h_1 = 1 \cdot 10^{-5}$, $h_2 = 2 \cdot 10^{-3}$, $h_3 = 2 \cdot 10^{-2}$, $h_4 = 1 \cdot 10^{-4}$, respectively.

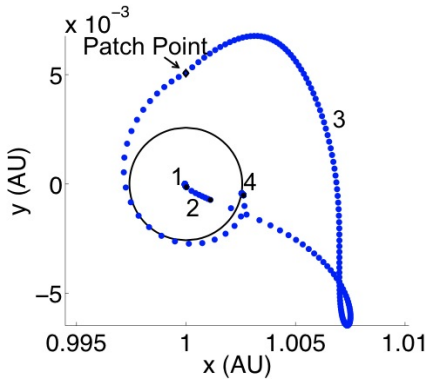

Figure 8 Sections of Initial Guess 1. The trajectory is divided into four sections of uniform step size ensuring that the trajectory consists of sufficient nodes near the Earth and Moon to capture the dynamics but few enough total nodes for reasonable computation time using *Matlab*.

Feasible Trajectories

For DMOC, the state q includes (x, y) and represents the x- and y-position of the trajectory. The Lagrangian describing the bicircular 4-body model is

$$L = \frac{1}{2}\left(\dot{x}^2 + \dot{y}^2\right) + \frac{1}{2}\left(x^2 + y^2\right) + x\dot{y} - y\dot{x} + \frac{\mu_E}{\sqrt{(x - x_E)^2 + y^2}} + \frac{\mu_S}{\sqrt{(x - x_S)^2 + y^2}} + \frac{\mu_M}{\sqrt{(x - x_M)^2 + (y - y_M)^2}} \tag{30}$$

The control force, $f(q, \dot{q}, u) = u$, consisting of the control parameters (u_x, u_y) represents the control force in the x- and y-direction, respectively. The next step before the optimization is the formulation of a feasible trajectory. By definition, a feasible trajectory is a solution that satisfies the dynamics of the system and desired boundary conditions but is not optimal. To create a feasible trajectory, DMOC is applied with the cost function set to one, allowing DMOC to adjust the optimization variables to fulfill the constraints. The constraints require that the forced discrete Euler-Lagrange equations are fulfilled (enforcing the dynamics), the initial altitude orbit about the Earth must be 206.9 km, and the final altitude at the Moon must be 326.8 km. These numbers were chosen to match those of IG1. Also, the initial and final radial velocity must be zero. Now, this procedure is applied to IG1 and IG2 in two different ways. For the first case, the flight time is held constant and the resulting trajectories are called Feasible FFT1 and FFT2 (Fixed Flight Time). For the second case, another optimization variable, λ, is introduced that allows the flight time to be adjusted by DMOC. $\lambda \in [0.01, 1.5]$ is a scaling factor and is applied to the step size in section 4; that is, $h_{4_{new}} = \lambda h_4$. Since each section consists of a constant number of nodes, variation of the step size changes the final time. Feasible trajectories created using this modification are denoted Feasible VFT1 and Feasible VFT2 (Variable Flight Time). Figure 9 shows each of the feasible trajectories,

and Figure 10 shows the time evolution of the control magnitude $U = \sqrt{u_x^2 + u_y^2}$, for each trajectory. Note that the control profile does not include ΔV_E and ΔV_M. Also, notice that for Feasible FFT2 and Feasible VFT2, there is a second spike in addition to the one representing the impulsive ΔV at the patch point. This impulse is added by DMOC to fulfill the final altitude condition at the Moon, reducing the final altitude from 16,228 km for the initial guess to 326 km for the feasible trajectory. Table 2 displays the flight time and ΔV for each of the feasible trajectories.

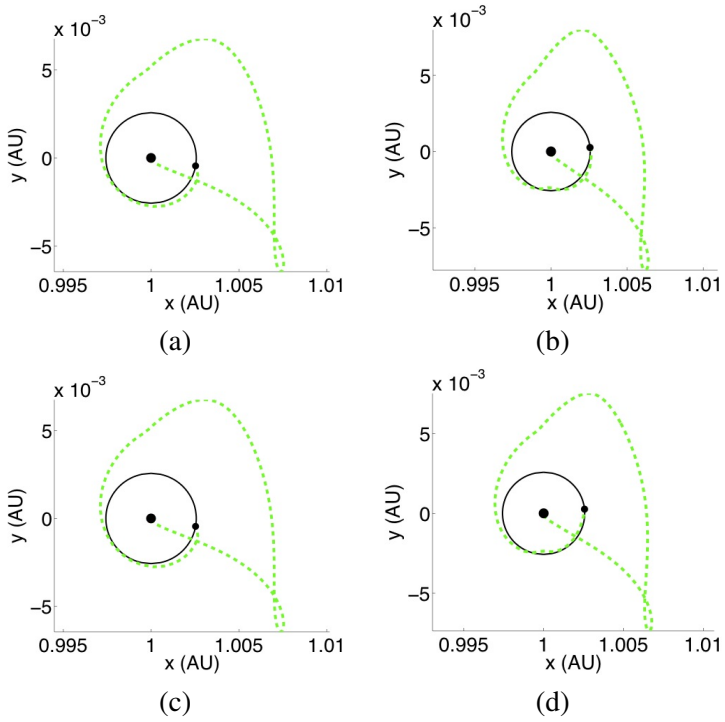

Figure 9 Feasible trajectories with fixed flight time (FFT) and variable flight time (VFT): a) Feasible FFT1, Total $\Delta V = 3,759.8$ m/s, b) Feasible FFT2, Total $\Delta V = 3,970.0$ m/s, c) Feasible VFT1, Total $\Delta V = 3,759.8$ m/s, and d) Feasible VFT2, Total $\Delta V = 3,864.0$ m/s.

Table 2. Details of Feasible Trajectories

	Feasible FFT1	Feasible FFT2	Feasible VFT1	Feasible VFT2
Flight Time (days)	175.5	178.8	175.5	178.8
Total ΔV (m/s)	3,759.8	3,970.0	3,759.8	3,864.0
ΔV_E (m/s)	2,931.4	3,028.0	2,931.4	3,028.0
ΔV_M (m/s)	631.3	644.0	631.3	632.9
ΔV_{traj} (m/s)	197.2	298.0	197.2	203.1

Optimization

Now, the feasible trajectories are used as initial guesses for the full DMOC optimization. For optimization with fixed flight time (FFT), the discrete cost function is

$$J_d(u_d) = h_1\|(u_1)_d\| + h_2\|(u_2)_d\| + h_3\|(u_3)_d\| + h_4\|(u_4)_d\| + \alpha\delta V_M \tag{31}$$

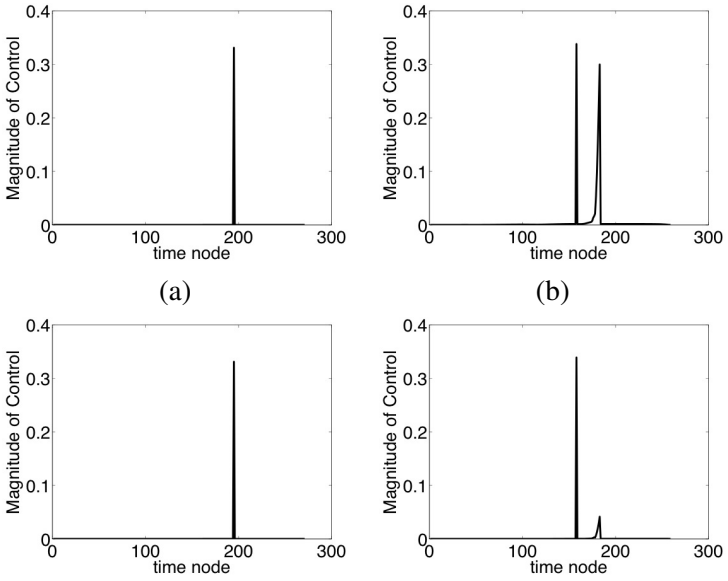

Figure 10 Control magnitude for feasible trajectory (excluding ΔV_E and ΔV_M): a) Feasible FFT1, b) Feasible FFT2, c) Feasible VFT1, and d) Feasible VFT2.

where $(u_i)_d = \{(u_{x,i}, u_{y,i})_k\}_{k=0}^{N_i-1}$ is a vector of length $2N_i$ with $N_i + 1$ being the number of discretization points in section i, $i = 1, \ldots, 4$, $\|\cdot\|$ denotes the 2-norm, α is a scaling factor (10^{-2} for this case), and δV_M is the dimensionless ΔV needed to insert the spacecraft into a circular orbit at the final altitude in the normalized coordinates of the Sun-Earth rotating frame. α reduces the order of magnitude of δV_M so that the order of magnitude of each of the terms in the cost function is the same. Without this scaling factor, δV_M is much larger than the other terms in Eq. (31), and it dominates the optimization. The ΔV applied throughout the trajectory, based on the control forces computed with DMOC, is computed as follows

$$\Delta V_{traj} = \alpha_V \left(h_1\|(u_1)_d\| + h_2\|(u_2)_d\| + h_3\|(u_3)_d\| + h_4\|(u_4)_d\|\right) \tag{32}$$

where α_V scales the velocity to m/s units.

The constraints are the same as for the feasible trajectories. In addition, the magnitude of the velocity at the first node (closest to the Earth) must match that of the corresponding feasible trajectory. This constraint helps with the convergence.

For optimization with variable flight time (VFT), the cost function is

$$J_d(u_d) = h_1\|(u_1)_d\| + h_2\|(u_2)_d\| + h_3\|(u_3)_d\| + h_{4_{new}}\|(u_4)_d\| + \alpha\delta V_M + \beta\lambda T \tag{33}$$

where T is the flight time in days, α is the same scaling factor as before, and $\beta = 10^{-4}$ is a scaling factor for the flight time. In addition to the constraints used for the fixed flight time optimization, the direction of velocity at the first node is required to match that of the first node of the feasible trajectory.

OPTIMIZATION RESULTS

DMOC is run using the feasible trajectories FFT1, FFT2, VFT1, and VFT2 as initial guesses, leading to the locally optimal trajectories Optimal FFT1, Optimal FFT2, Optimal VFT1, and Op-

timal VFT2, respectively. The trajectories are shown in Figure 11 and the flight time and ΔV are shown in Table 3.

Table 3. Details of Optimal Trajectories

	Optimal FFT1	Optimal FFT2	Optimal VFT1	Optimal VFT2
Flight Time (days)	175.5	178.8	175.3	178.4
Total ΔV (m/s)	3,569.6	3,663.8	3,242.7	3,363.2
ΔV_E (m/s)	2,931.4	3,028.0	2,931.4	3,028.0
ΔV_M (m/s)	632.8	632.7	304.5	330.5
ΔV_{traj} (m/s)	5.5	3.1	6.8	4.7

In Figure 11, it is clear that each optimal trajectory follows the general shape of the feasible trajectory used as the initial guess for DMOC, demonstrating the importance of the initial guess and the local nature of the solutions. In Table 3, notice ΔV_{traj}. For the feasible trajectories, ΔV_{traj} is 197.2 m/s, 298 m/s, 197.2 m/s, and 203.1 m/s for Feasible FFT1, FFT2, VFT1, and VFT2, respectively, and is concentrated primarily in one or two impulses. Compare that impulsive control profile with those shown in Figure 12. The control for the optimal trajectories is spread out over the entire trajectories with smaller magnitude. ΔV_{traj} is reduced to just 5.5 m/s, 3.1 m/s, 6.8 m/s, and 4.7 m/s for Optimal FFT1, FFT2, VFT1, and VFT2, respectively. Now, note the similarity between Optimal FFT1 and Optimal FFT2. Even though the first initial guess for Optimal FFT2 (IG2) did not end close enough to the Moon, DMOC still finds a good optimal solution that fulfills the constraints and final altitude requirements. However, since IG1 does fulfill the final altitude requirement, the total ΔV of Optimal FFT1 is slightly better than Optimal FFT2. When comparing the fixed flight time results to the variable final time results, two things are important. Obviously, the flight times are different, but only slightly. More noticeable is the difference in ΔV_M. The variability of the flight time enables the final position of the Moon to change, allowing DMOC to find a trajectory with a smaller ΔV to move into circular orbit about the Moon. However, even though ΔV_M is smaller for Optimal VFT1 and VFT2, the ΔV_{traj} is just slightly higher.

Next we compare these results to the ΔV required using the Hohmann transfer method. As shown in Figure 13, the Hohmann transfer consists of two ΔV: ΔV_1 is required to move from the initial circular Earth orbit onto the transfer ellipse. Then, ΔV_2 moves the spacecraft from the transfer ellipse onto a circular orbit that follows the Moon, at the desired altitude, in rotation around the Earth. Note that the ΔV required for circular orbit insertion about the Moon is not included in these calculations. Table 4 shows the percentage improvement of the DMOC optimal solution over the Hohmann transfer method. The DMOC optimal trajectories, Optimal VFT1 and FFT1, produce the best results, moving from Earth orbit to the Moon using 25.8% less ΔV than the Hohmann transfer. While the optimal trajectories use much less ΔV, the travel time is much longer. On average, a Hohmann transfer takes approximately 5 days to reach the Moon. As shown in Table 3, a spacecraft following one of the trajectories from Figure 11 would travel for 175 - 178 days before reaching the Moon. Therefore, these type of trajectories are best suited for missions in which flight time is not critical.

Furthermore, how do the DMOC results fit in the context of other Moon missions? Table 5 presents the results for 3 missions (SMART-1, Hiten, Shoot the Moon), as well as the best DMOC result for Optimal VFT1. The table includes details about the ΔV, initial and final orbit conditions, and flight time. The ΔV are described in the same manner as the DMOC optimization results. Since the ion thrusters apply small thrust throughout SMART-1's trajectory, only the total ΔV is given.

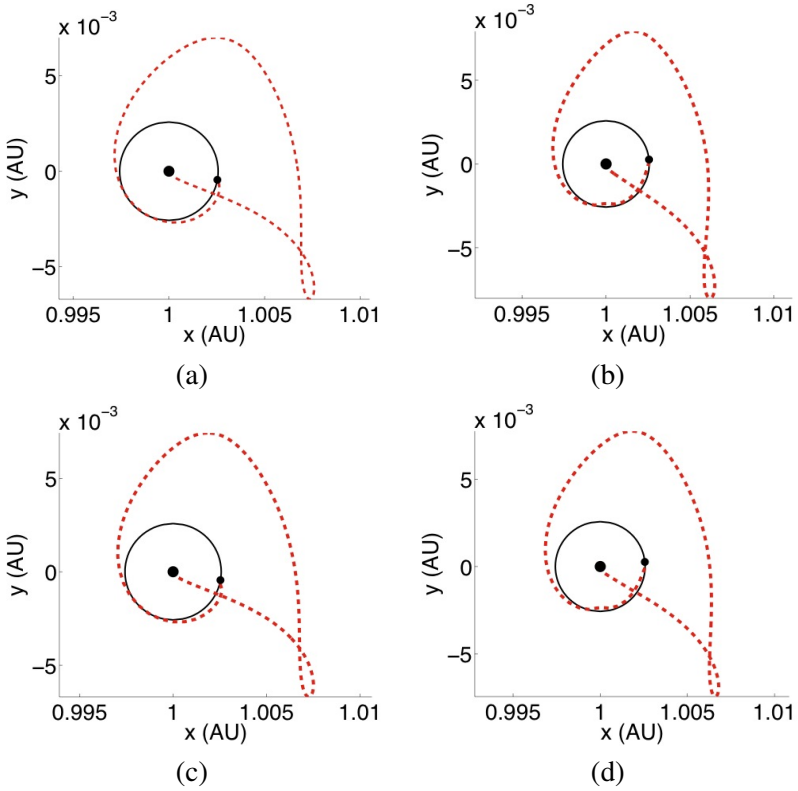

Figure 11 Optimal trajectories for a) Optimal FFT1, Total $\Delta V = 3,569.6$ m/s with $\Delta V_{traj} = 5.5$ m/s, b) Optimal FFT2, Total $\Delta V = 3,663.8$ m/s with $\Delta V_{traj} = 3.1$ m/s, c) Optimal VFT1, Total $\Delta V = 3,242.7$ m/s with $\Delta V_{traj} = 6.8$ m/s, and d) Optimal VFT2, Total $\Delta V = 3,363.2$ m/s with $\Delta V_{traj} = 4.7$ m/s.

Table 4. DMOC versus Hohmann Transfer: Total ΔV Percentage Improvement

	% Improvement
Optimal FFT1	25.8%
Optimal FFT2	23.4%
Optimal VFT1	25.8%
Optimal VFT2	23.4%

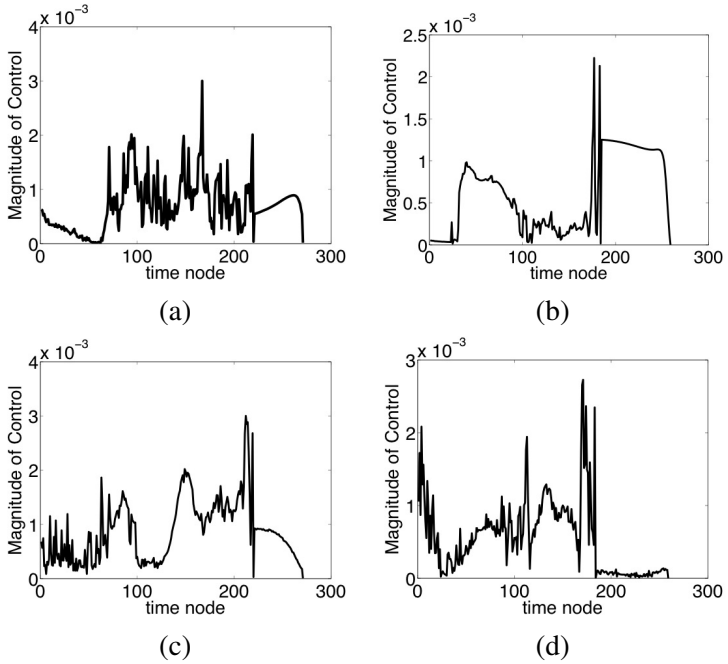

Figure 12 Optimal control magnitude for optimal trajectory (excludes ΔV_E and ΔV_M): a) Optimal FFT1, b) Optimal FFT2, c) Optimal VFT1, and d Optimal VFT2)

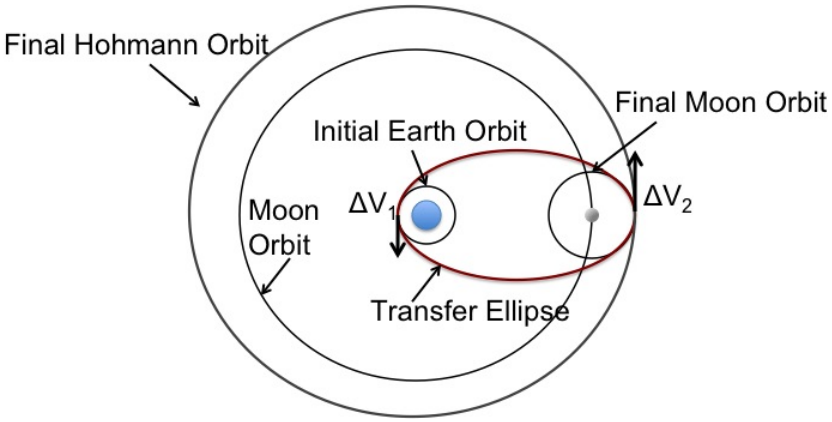

Figure 13 Hohmann Transfer: spacecraft travels from circular Earth orbit to Moon via transfer ellipse.

The Hiten mission's ΔV is broken into three impulsive thrusts, just like for the initial trajectories designed using invariant manifolds of the 3-body problem. The first, ΔV_E, is applied at the beginning to move from the initial orbit, an elliptical phasing orbit, onto the trajectory. ΔV_{traj} is applied at a point nearly four times the Moon's orbital radius from Earth, allowing natural ballistic capture. At the end, ΔV_M is applied to enter the final circular orbit. For Shoot the Moon,[12] ΔV_E moves the spacecraft from circular Earth orbit onto the trajectory, and ΔV_{traj} is applied mid-course to facilitate ballistic capture. There is no final maneuver for a lunar orbit. The ΔV of these missions cannot be directly compared since the boundary conditions and orbits involved are completely different. The trajectories for Hiten, Shoot the Moon, and DMOC look similar, so they are more comparable to each other than SMART-1, which is very different. However, some general conclusions may be drawn. First, using DMOC greatly reduces ΔV_{traj} compared to that of Hiten and Shoot the Moon. DMOC's distributed control profile is much more efficient than a single impulse as used by Hiten and Shoot the Moon. Also, note that starting in an elliptical orbit, like Hiten's, results in a significantly smaller ΔV_E than starting in a circular orbit like Shoot the Moon and DMOC Optimal VFT1.

Table 5. Moon Mission Results

Mission	ΔV (m/s)	Earth Orbit (km)	Moon Orbit (km)	Flight Time (days)
SMART-1	$\Delta V_{total} = 3,500$	GTO $r_p = 654$ $r_a = 35,885$	Polar $r_p = 300 - 450$ $r_a = 3,000$	505
Hiten	$\Delta V_E = 14$ $\Delta V_{traj} = 30$ $\Delta V_M = 648$	Elliptical $r_p = 8,900$ $r_a \approx 450,000$	Circular $r = 100$	150
Shoot the Moon	$\Delta V_E = 3,211$ $\Delta V_{traj} = 34$	Circular $r = 200$	Ballistic capture	180
DMOC Optimal VFT1	$\Delta V_E = 2,931.4$ $\Delta V_{traj} = 6.8$ $\Delta V_M = 304.5$	Circular $r = 206.9$	Circular $r = 326.8$	175.3

Also, it is important to note that the DMOC optimal trajectories are approximations to real trajectories. Application of more advanced design software, such as the tools used at JPL, is necessary to extend these trajectories to fully integrated trajectories with ephemeris.

CONCLUSION AND FUTURE WORK

Invariant manifolds of two PCR3BPs are successfully used to develop an initial guess for the optimization of a low ΔV trajectory in the 4-body system. Using DMOC, it is possible to reduce the large ΔV of 3,759.8 m/s necessary to reach the moon along the feasible trajectory, Feasible VFT1, to just 3,242.7 m/s along the optimal trajectory, Optimal VFT1. Also, DMOC reduces the ΔV required along the trajectory from 197.2 m/s to just 6.8 m/s. Now that the combination of invariant manifold techniques and DMOC is shown to be viable, the method could be applied to other design problems.

For the shoot the moon problem, an adaptive time-stepping strategy for DMOC would provide a huge benefit and is also essential for other problems in space mission design, e.g. the trajectories require a finer time-stepping near planets due to the strong influence of gravity, while for a transfer

in nearly free space, only a few discretization points are necessary to accurately reflect the dynamics of the system. Here, different strategies such as error control based on the discretization grid under consideration[24] and variational approaches[33] could be investigated.

In addition, since DMOC results are locally optimal, dependent on initial guess, further investigation leading to globally optimal solutions is desirable. Kobilarov (2008)[34] combines DMOC with sampling-based roadmaps to compute near globally optimal solutions for various problems including a helicopter traveling through an urban environment towards a goal state. This motion planning method begins by compiling a library of DMOC primitives (short, optimal paths from a start state to an intermediate goal state). Then, a sampling-based roadmap strategy (e.g. probabilistic roadmaps) combines these DMOC primitives into a full trajectory that reaches the goal state. The use of DMOC primitives depends on the invariance of the dynamics under some group action.[34] Due to the time-dependent nature of the dynamics of the 4-body problem, DMOC primitives most likely will not be applicable for this problem. However, a similar strategy may successfully lead to globally optimal trajectories in the 4-body problem. One idea is to apply probabilistic roadmaps to create a mesh along the state space of the invariant manifolds of the PCR3BP, and then DMOC will be used to connect points on the mesh from the start state to goal state, minimizing the necessary control.

ACKNOWLEDGMENT

The authors would like to acknowledge Dr. Shane Ross for his help with the Shoot the Moon problem and invariant manifolds, as well as Dr. Marin Kobilarov, Stefano Campagnola, and Evan Gawlik for many useful discussions. Also, many thanks to Dr. Gregory Whiffen for his help with JPL's design tools. This research was partly supported by a National Defense Science and Engineering Graduate (NDSEG) Fellowship and the AFOSR grant FA9550-08-1-0173.

REFERENCES

[1] E. A. Belbruno and J. Miller, "Sun-perturbed Earth-to-Moon Transfers with Ballistic Capture," *Journal of Guidance, Control, and Dynamics*, Vol. 16, No. 4, 1993, pp. 770–775.

[2] E. Belbruno, *Capture Dynamics and Chaotic Motions in Celestial Mechanics*. Princeton University Press, 2004.

[3] O. Camino, M. Alonso, R. Blake, D. Milligan, J. d. Bruin, and S. Ricken, "SMART-1: Europe's Lunar Mission Paving the Way for New Cost Effective Ground Operations (RCSGSO)," *6th International Symposium "Reducing the Costs of Spacecraft Ground Systems and Operations (RCSGSO)"*, ESA/ESOC, Darmstadt, Germany, 2005.

[4] C. Conley, "Low Energy Transit Orbits in the Restricted Three-Body Problem," *SIAM J. Appl. Math*, Vol. 16, 1968, pp. 732–746.

[5] R. McGehee, *Some Homoclinic Orbits for the Restricted Three-Body Problem*. PhD thesis, University of Wisconsin, 1969.

[6] G. Gómez, A. Jorba, J. Masdemont, and C. Simó, "Study of the Transfer From the Earth to a Halo Orbit Around the Equilibrium Point L_1," *Celestial Mechanics and Dynamical Astronomy*, Vol. 56, 1993, pp. 541–562.

[7] G. Gómez, W. Koon, M. Lo, J. E. Marsden, J. Masdemont, and S. D. Ross, "Invariant Manifolds, The Spatial Three-Body Problem and Space Mission Design," *Astrodynamics Specialist Conference*, AAS/AIAA, 2001.

[8] W. Koon, M. Lo, and J. E. Marsden, "The Genesis Trajectory and Heteroclinic Connections," *Astrodynamics*, Vol. 103, 1999, pp. 2327–2343.

[9] G. Gómez, W. Koon, M. Lo, J. E. Marsden, J. Masdemont, and S. D. Ross, "Connecting Orbits and Invariant Manifolds in the Spatial Three-Body Problem," *Nonlinearity*, Vol. 17, 2004, pp. 1571–1606.

[10] M. Dellnitz, O. Junge, M. W. Lo, and B. Thiere, "On the Detection of Energetically Efficient Trajectories for Spacecraft," *AAS/AIAA Astrodynamics Specialist Conference*, Quebec City, Paper AAS, 01-326, 2001.

[11] W. S. Koon, M. W. Lo, J. E. Marsden, and S. D. Ross, "Low Energy Transfer to the Moon," *Celestial Mechanics and Dynamical Astronomy*, Vol. 81, No. 1-2, 2001, pp. 63–73.

[12] W. S. Koon, M. W. Lo, J. E. Marsden, and S. D. Ross, "Shoot the Moon," *Spaceflight Mechanics*, Vol. 105, No. 2, 2000, pp. 1017–1030.

[13] M. Dellnitz, S. Ober-Blöbaum, M. Post, O. Schütze, and B. Thiere, "A Multi-objective Approach to the Design of Low Thrust Space Trajectories Using Optimal Control," Submitted to *Celestial Mechanics and Dynamical Astronomy*, 2008.

[14] M. Dellnitz, O. Junge, M. Post, and B. Thiere, "On Target for Venus—Set Oriented Computation of Energy Efficient Low Thrust Trajectories," *Celestial Mechanics & Dynamical Astronomy.*, Vol. 95, No. 1-4, 2006, pp. 357–370.

[15] O. Junge, J. E. Marsden, and S. Ober-Blöbaum, "Discrete Mechanics and Optimal Control," *Proceedings of the 16th IFAC World Congress*, 2005.

[16] J. Stoer and R. Bulirsch, *Introduction into Numerical Analysis*. 2nd ed., Springer, 1993.

[17] D. Kraft, "On Converting Optimal Control Problems Into Nonlinear Programming Problems," *Computational Mathematical Programming* (K. Schittkowsky, ed.), Vol. F15 of *NATO ASI series*, pp. 261–280, Springer, 1985.

[18] G. Hicks and W. Ray, "Approximation Methods for Optimal Control Systems," *Can. J. Chem. Engng.*, Vol. 49, 1971, pp. 522–528.

[19] P. Deuflhard, "A Modified Newton Method for the Solution of Ill-conditioned Systems of Nonlinear Equations with Application to Multiple Shooting," *Numerische Mathematik*, Vol. 22, 1974, pp. 289–315.

[20] H. G. Bock and K. J. Plitt, "A Multiple Shooting Algorithm for Direct Solution of Optimal Control Problems," *9th IFAC World Congress*, Budapest, Hungary, Pergamon Press, 1984, pp. 242–247.

[21] D. Leineweber, I. Bauer, H. Bock, and J. Schlöder, "An Efficient Multiple Shooting Based Reduced SQP Strategy for Large-scale Dynamic Process Optimization. Part I: Theoretical Aspects," *Comp. Chem. Eng.*, Vol. 27, 2003, pp. 157–166.

[22] O. v. Stryk, "Numerical Solution of Optimal Control Problems By Direct Collocation," *Optimal Control - Calculus of Variation, Optimal Control Theory and Numerical Methods* (R. Bulirsch, A. Miele, J. Stoer, and K. H. Well, eds.), Vol. 111 of *International Series of Numerical Mathematics*, pp. 129–143, Birkhäuser, 1993.

[23] L. T. Biegler, "Solution of Dynamic Optimization Problems By Successive Quadratic Programming and Orthogonal Collocation," *Computers and Chemical Engineering*, Vol. 8, 1984, pp. 243–248.

[24] J. T. Betts, "Survey of Numerical Methods for Trajectory Optimization," *AIAA J. Guidance, Control, and Dynamics*, Vol. 21, No. 2, 1998, pp. 193–207.

[25] T. Binder, L. Blank, H. G. Bock, R. Bulirsch, W. Dahmen, M. Diehl, T. Kronseder, W. Marquardt, J. P. Schlöder, and O. v. Stryk, "Introduction to Model Based Optimization of Chemical Processes on Moving Horizons," *Online Optimization of Large Scale Systems: State of the Art* (M. Grötschel, S. O. Krumke, and J. Rambau, eds.), pp. 295–340, Springer, 2001.

[26] S. Ober-Blöbaum, *Discrete Mechanics and Optimal Control*. PhD thesis, University of Paderborn, 2008.

[27] J. E. Marsden and M. West, "Discrete Mechanics and Variational Integrators," *Acta Numerica*, Vol. 10, 2001, pp. 357–514.

[28] P. E. Gill, W. Murray, and M. A. Saunders, "SNOPT: An SQP Algorithm for Large-scale Constrained Optimization," Report NA 97-2, Department of Mathematics, University of California, San Diego, CA, USA, 1997.

[29] P. E. Gill, L. O. Jay, M. W. Leonard, L. R. Petzold, and V. Sharma, "An SQP Method for the Optimal Control of Large-scale Dynamical Systems," *J. Comp. Appl. Math*, Vol. 20, 2000, pp. 197–213.

[30] M. J. D. Powell, "A Fast Algorithm for Nonlinearly Constrained Optimization Calculations," *Numerical Analysis* (G. A. Watson, ed.), Vol. 630 of *Lecture Notes in Mathematics*, pp. 261–280, Springer, 1978.

[31] S. P. Han, "Superlinearly Convergent Variable-metric Algorithms for General Nonlinear Programming Problems," *Mathematical Programming*, Vol. 11, 1976, pp. 263–282.

[32] S. D. Ross, *Cylindrical Manifolds and Tube Dynamics in the Restricted Three-Body Problem*. PhD thesis, California Institute of Technology, 2004.

[33] L. Kharevych, P. Mullen, S. Leyendecker, Y. Tong, J. E. Marsden, and M. Desbrun, "Robust Time-adaptive Integrators for Computer Animation," In preparation, 2008.

[34] M. Kobilarov, *Discrete Geometric Motion Control of Autonomous Vehicles*. PhD thesis, University of Southern California, August 2008.